

Gas phase analogs of stable sodium-tin Zintl ions: Anion photoelectron spectroscopy and electronic structure

W.-J. Zheng,¹ O. C. Thomas,¹ J. M. Nilles,¹ K. H. Bowen,^{1,a)} A. C. Reber,²
and S. N. Khanna²

¹*Departments of Chemistry and Materials Science, Johns Hopkins University, Baltimore, Maryland 21218, USA*

²*Department of Physics, Virginia Commonwealth University, Richmond, Virginia 23284, USA*

(Received 15 April 2011; accepted 17 May 2011; published online 13 June 2011)

Mass spectrometry and photoelectron spectroscopy together with first principles theoretical calculations have been used to study the electronic and geometric properties of the following sodium-tin, cluster anion/neutral cluster combinations, $(\text{Na}_n\text{Sn}_4)^{-(n-4)}$, $n = 0-4$ and $(\text{NaSn}_m)^{-(m-1)}$, $m = 4-7$. These synergistic studies found that specific Zintl anions, which are known to occur in condensed Zintl phases, also exist as stable moieties within free clusters. In particular, the cluster anion, $(\text{Na}_3\text{Sn}_4)^-$ is very stable and is characterized as $(\text{Na}^+)_3(\text{Sn}_4)^{-4}$; its moiety, $(\text{Sn}_4)^{-4}$ is a classic example of a Zintl anion. In addition, the cluster anion, $(\text{NaSn}_5)^-$ was the most abundant species to be observed in our mass spectrum, and it is characterized as $\text{Na}^+(\text{Sn}_5)^{2-}$. Its moiety, $(\text{Sn}_5)^{2-}$ is also known to be present as a Zintl anion in condensed phases. © 2011 American Institute of Physics. [doi:10.1063/1.3597604]

I. INTRODUCTION

The term, Zintl anion, refers to the family of multiply charged polyatomic anions formed by the heavier (and mildly electronegative) post-transition elements.¹ Zintl anions can combine with cations of highly electropositive elements, such as alkali metals, to form solids and “melts” which are usually referred to as Zintl phases. Among the simpler types of Zintl phases are the 1:1 MTt compounds, e.g., those formed between $M = \text{Na}, \text{K}, \text{Rb},$ and Cs and Tt (tetrel) = $\text{Ge}, \text{Sn},$ and Pb . These compounds are known to contain tetrahedra, Tt_4 , and they are typically described as $(M^+)_4(\text{Tt}_4)^{4-}$, depicting the interaction of four cations with a single, multiply charged polyatomic Zintl anion. While it is generally assumed that ionic bonding dominates, the bonding in Zintl phases can be complicated, and there is thought to be a substantial degree of covalent character present as well.²⁻⁴

While most studies of Zintl phases have been conducted in the solid state, there is a growing body of work in the gas phase as well. Almost twenty years ago, gas phase Zintl anions were identified through magic numbers in the mass spectra of sodium/bismuth clusters, e.g., the presence of the $(\text{Bi}_3)^{3-}$ Zintl anion was inferred from the observation of $(\text{Na}_4\text{Bi}_3)^+$ as a magic number species.^{5,6} Around the same time, the presence of Zintl anions were also inferred from the results of the photoionization mass spectral studies of III-V and IV-V intermetallic clusters.^{7,8} More recently, the presence of Zintl anions, such as $(\text{Al}_4)^{2-}$, $(\text{Ga}_4)^{2-}$, and $(\text{In}_4)^{2-}$ has been inferred within gas phase anions, such as $(\text{NaGa}_4)^-$. Photoelectron experiments supported by theoretical calculations showed that these Zintl anions exhibit square planar geometries and aromatic character.^{9,10} Over the past few years, however, a veritable landslide of gas phase Zintl anion activity has

occurred. Endohedral Zintl anions, such as $[\text{Pt}@\text{Pb}_{12}]^{2-}$ and $[\text{Ni}@\text{Pb}_{10}]^{2-}$, have been synthesized in the condensed phase and laser desorbed into the gas phase as singly charged anions from their salts.^{11,12} The long-predicted¹³ ionic bonding character of KAl_{13} , i.e., K^+ and the singly charged “Zintl” anion, $(\text{Al}_{13})^-$, was confirmed by photoionization¹⁴ and anion photoelectron experiments.¹⁵⁻¹⁷ The viability of Zintl anions, such as $(\text{Sn}_{12})^{2-}$ and $(\text{Pb}_{12})^{2-}$, was revealed through calculations and anion photoelectron spectra of $(\text{KSn}_{12})^-$ and $(\text{KPb}_{12})^-$, respectively.^{18,19} Even more recently, Zintl analogs of Sn_n^{2-} have been synthesized in the gas phase by doping with elements of different valence to study the electronic structure and stability of isoelectronic species.²⁰ Furthermore, a protocol for identifying and characterizing clusters with potential for cluster assembly has been proposed using K_nAs_m Zintl clusters as an example system.²¹ An exciting aspect of this topic is the prospect of building extended ionic lattices based on intact Zintl anion units and one or more cations in order to achieve charge neutrality and to meet packing requirements.

Among Zintl phases, the 1:1 sodium/tin system, $(\text{Na}^+)_4(\text{Sn}_4)^{-4}$, has been particularly well studied. The $(\text{Sn}_4)^{-4}$ Zintl anion has a tetrahedral structure in the solid state and is isoelectronic with the tetrahedral pnictide cages of P_4 and Sb_4 . Exploiting the isoelectronic argument still further, some theoretical investigators²² have suggested that the pseudo-aromatic character found in Sb_4 should also be present in $(\text{Sn}_4)^{-4}$. Results from other theoretical studies have shown that the structure of Sn_4 evolves from a planar rhombus toward a tetrahedron as extra electrons are added to it, and that the structure of Na_4Sn_4 can be described as a Sn_4 tetrahedron sitting inside an opposed Na_4 tetrahedron.^{23,24} In addition, experimental measurements in the solid state²⁵ and the complementary band structure calculations²⁶ show that the sodium/tin Zintl phase is a semiconductor at cryogenic temperatures. There, tetrahedral $(\text{Sn}_4)^{4-}$ polyanions sit

^{a)} Author to whom correspondence should be addressed. Electronic mail: kbowen@jhu.edu.

in a body-centered tetragonal lattice. As expected, however, the sodium/tin alloy evolves from a semiconductor toward a metallic liquid phase with increasing temperature. Even then, however, the alloy's $(\text{Sn}_4)^{4-}$ Zintl anions survive intact, although at still higher temperatures, rapid reorientations of $(\text{Sn}_4)^{4-}$ polyanions and migrations of Na^+ cations occur.²⁷

In the present joint experimental/theoretical work, we study the anions and corresponding neutrals from two, gas-phase sodium/tin cluster series, $(\text{Na}_n\text{Sn}_4)^-/\text{Na}_n\text{Sn}_4$, $n = 0-4$ and $(\text{NaSn}_m)^-/\text{NaSn}_m$, $m = 4-7$. In the former series, we consider the structural and electronic progressions taking place in $(\text{Sn}_4)^{-x}$ sub-units as their negative charges are gradually increased through successive addition of alkali atoms. Not only do the sodium atoms supply electrons, but upon releasing their valence electrons, they become cations which stabilize multiply charged $(\text{Sn}_4)^{-x}$ anionic sub-units much as counter-cations stabilize Zintl anions in condensed phases against Coulomb explosion. In the latter stoichiometric series, we consider the structural and electronic changes taking place as the number of tin atoms are varied, focusing on $(\text{NaSn}_5)^-$ and its special stability.

The experimental side of this work uses mass spectrometry and anion photoelectron spectroscopy as its tools, while the theoretical side employs density functional theory at the level of the generalized gradient approximation. Anion photoelectron spectra provide electron affinities, vertical detachment energies, and electronic state splittings. For cases where the anion has a doublet ground state while the neutral is a singlet, the spectra also provides information on the highest occupied molecular orbital (HOMO)-lowest unoccupied molecular orbital (LUMO) gaps for the anions' corresponding neutrals. Theoretical calculations supply geometric structures for the anions and their corresponding neutrals as well as the electron affinities and electronic state splittings, again including HOMO-LUMO gaps, for the neutrals.

II. METHODS

A. Experimental

Negative ion photoelectron (photodetachment) spectroscopy is conducted by crossing a mass-selected beam of negative ions with a fixed-frequency photon beam and analyzing the energies of the resultant photodetached electrons. This technique is a direct approach to measure electron binding energies, and it is governed by the energy-conserving relationship, $h\nu = \text{EBE} + \text{EKE}$, where $h\nu$ is the photon energy, EBE is the electron binding (transition) energy, and EKE is the measured electron kinetic energy. Briefly, both mass spectra and photoelectron spectra are collected using an apparatus consisting of a laser vaporization source employing a Nd:YAG laser, a linear time-of-flight mass spectrometer for mass analysis and selection, a second Nd:YAG laser for photodetachment, and a magnetic bottle for electron energy analysis (resolution = 35 meV at EKE = 1 eV). Further details about our apparatus are given Ref. 28.

Tin/sodium cluster anions were generated in the laser vaporization source by focusing a pulsed laser onto a sodium-coated tin rod (0.25 in. diameter, 5N purity, electronic speckle

pattern interferometry (ESPI)). The tin rod had been previously coated with a thin layer of sodium by evaporating sodium from a small oven under the rod. Second harmonic light (2.33 eV photons) from a Nd:YAG laser was employed for laser vaporization. The target rod was continuously rotated and translated by a motor to allow the laser to strike a different spot each time it fired. Simultaneously, a pulsed valve injected high pressure bursts of high purity helium into the laser vaporization region of the source. Size-selected sodium/tin cluster anions were photodetached with 3.49 eV photons.

B. Computational

The theoretical investigations were carried out using a density functional formalism²⁹ that incorporated exchange and correlation effects within the generalized gradient approximation functional proposed by Perdew *et al.*³⁰ Gaussian basis sets were employed to construct atomic wave functions, while the cluster wave functions were formed from linear combinations of atomic orbitals. The basis sets for Na included 6s, 4p, and 3d Gaussians, while the Sn had 8s, 7p, and 5d Gaussians. In each case, the basis set was supplemented by a diffuse Gaussian. The calculations were carried out using the Naval Research Laboratory Molecular Orbital Library set of codes developed by Pederson and co-workers.³¹⁻³³

For each cluster size, the geometry was optimized by starting from several initially selected configurations and then moving the atoms along the directions of sensed forces until the forces dropped below 10^{-3} hartree/a.u. The present studies compare calculated parameters with those derived from negative ion photoelectron spectra. In each case, we first studied the vertical transitions from the anion to its corresponding neutral species with the neutral species in the geometry of the anion. For example, starting from an anion cluster with a spin multiplicity of M, the transition energies to its neutral cluster counterparts in the geometry of the anion with multiplicities $M \pm 1$ were calculated. Since photodetachment processes are fast compared to ionic core relaxation times, these energies correspond to the electron binding energies of the peaks in the photoelectron spectra. However, since the electron from an anion can also originate from levels deeper than its HOMO, one also needs to consider the energies of the excited states for each of the multiplicities, $M \pm 1$. For these excited states, we calculated the total energies of the neutral clusters while forcing a vacancy in the appropriate orbital states corresponding to the electron ejected from the anionic clusters. Adiabatic electron affinities, which correspond to the energy difference between the ground state of a particular cluster anion and that of its optimized neutral counterpart, were also calculated.

III. RESULTS

A. Mass spectra

Figure 1 presents a typical mass spectrum of the anionic species generated in these experiments. The mass peaks are broadened due to tin's isotopic distribution. On the lower mass side of this spectrum the intensities of homogeneous

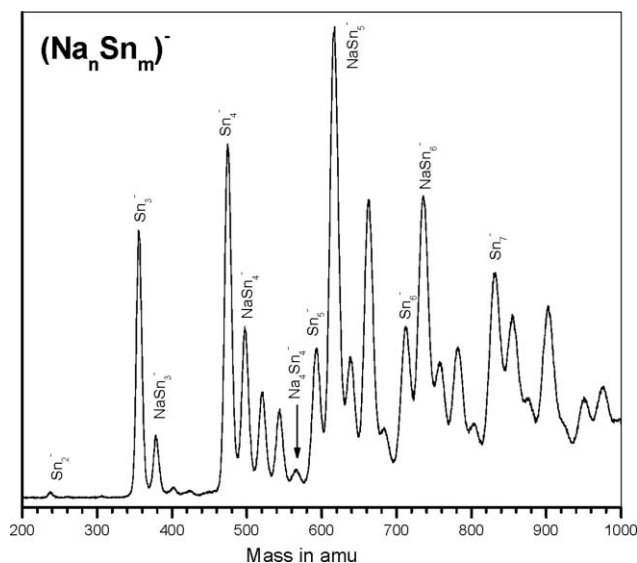


FIG. 1. Mass spectrum of the $(\text{Na}_n\text{Sn}_m)^-$ cluster anions generated in this study.

$(\text{Sn}_n)^-$ clusters are stronger than those of the heterogeneous sodium/tin cluster anions, whereas from the middle of the presented mass range on toward higher masses, the mixed sodium/tin cluster anion intensities begin to dominate. Several observations about the mass spectra foreshadow results from the photoelectron spectra and the calculations. For example, the anion intensities of the $(\text{Na}_n\text{Sn}_4)^-$ series decrease as n increases but with the intensity of $(\text{Na}_4\text{Sn}_4)^-$ showing a decrease that is even greater than the trend among the others. Also, among species in the $(\text{NaSn}_n)^-$ series, the intensity of $(\text{NaSn}_5)^-$ was observed to be especially abundant. In fact, it is the highest intensity peak in the mass spectrum. Furthermore, for $(\text{Na}_n\text{Sn}_m)^-$ species with $m \geq 5$, their intensities alternate between higher values when n is an odd number of sodium atoms and lower values when n is an even number. For example, the anion intensities of $(\text{NaSn}_5)^-$ and $(\text{Na}_3\text{Sn}_5)^-$ are greater than those of $(\text{Na}_2\text{Sn}_5)^-$ and $(\text{Na}_4\text{Sn}_5)^-$. Also, the intensities of $(\text{NaSn}_6)^-$ and $(\text{Na}_3\text{Sn}_6)^-$ are stronger than those of $(\text{Na}_2\text{Sn}_6)^-$ and $(\text{Na}_4\text{Sn}_6)^-$, and the intensities of $(\text{NaSn}_7)^-$ and $(\text{Na}_3\text{Sn}_7)^-$ are greater than those of $(\text{Na}_2\text{Sn}_7)^-$ and $(\text{Na}_4\text{Sn}_7)^-$.

B. Photoelectron spectra

The photoelectron spectra of $(\text{Na}_n\text{Sn}_4)^-$ ($n = 0-4$) cluster anions are presented in Fig. 2, while the photoelectron spectra of $(\text{NaSn}_m)^-$ ($m = 4-7$) cluster anions are shown in Fig. 3. The position of the peaks in each spectrum measure the electron binding energies of the photodetachment transitions from the ground vibronic state of that particular cluster anion to the ground and excited electronic states of that cluster anion's neutral counterpart. Theoretical studies indicate that the most stable configurations have the lowest spin multiplicity; all the anions examined are singlets, except for Sn_4^- , Na_2Sn_4^- , and Na_4Sn_4^- which are doublets. In each spectrum, vertical lines (stick spectra) indicate the vertical transition energies predicted by DFT calculations as described above. For

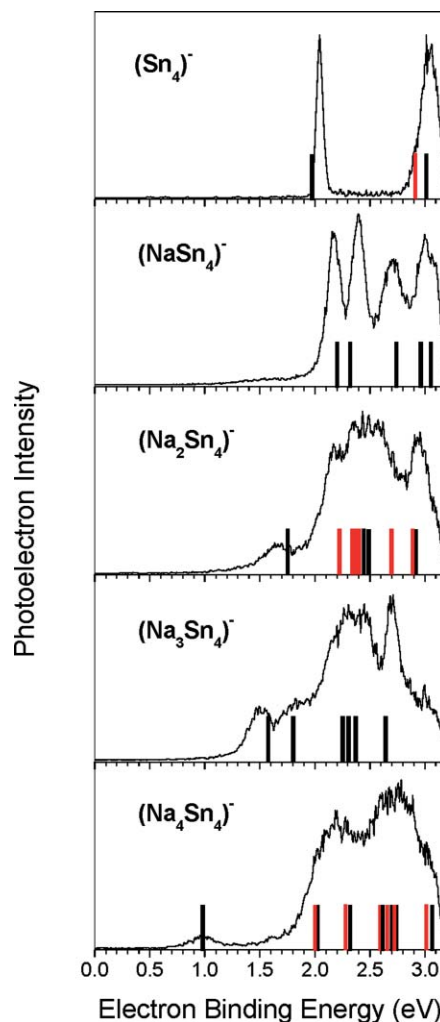


FIG. 2. Photoelectron spectra of $(\text{Na}_n\text{Sn}_4)^-$, $n = 0-4$. The stick spectra indicate the theoretically predicted vertical transitions, where black indicates transitions to the lowest spin multiplicity, and red indicates a transition to a triplet state. The clusters in which $n = 1$ and 3 are singlets, and in which $n = 0, 2$, and 4 are of doublet multiplicity.

anions with a doublet ground state, the dark lines represent transitions to the singlet neutral while the red lines correspond to transitions resulting in triplet neutral. For anions with singlet ground states, the dark lines represent transitions to neutral doublets. Table I provides a more direct comparison of the calculated and measured vertical detachment energies (VDE) and adiabatic electron affinities (AEA). Adiabatic electron affinity values of neutral species are numerically equivalent to adiabatic detachment energy (ADE) values of their corresponding anionic species. Electron affinity values were estimated to lie to the low EBE side of the center of lowest EBE peak (the VDE) in the photoelectron spectra, allowing for significant vibrational hot band contributions. (We estimate the anions' temperature at $\sim 200-300$ K.) Due to the width of the peaks and their significant tails, a more quantitative assessment was not feasible. In the Na_nSn_4 series, electron affinity values are seen to decrease steadily as n increases. Moreover, a maximum in the value of the HOMO-LUMO gap is seen at $n = 4$, i.e., on the order of 1 eV. A large HOMO-LUMO gap, such as this, is indicative of enhanced stability in the

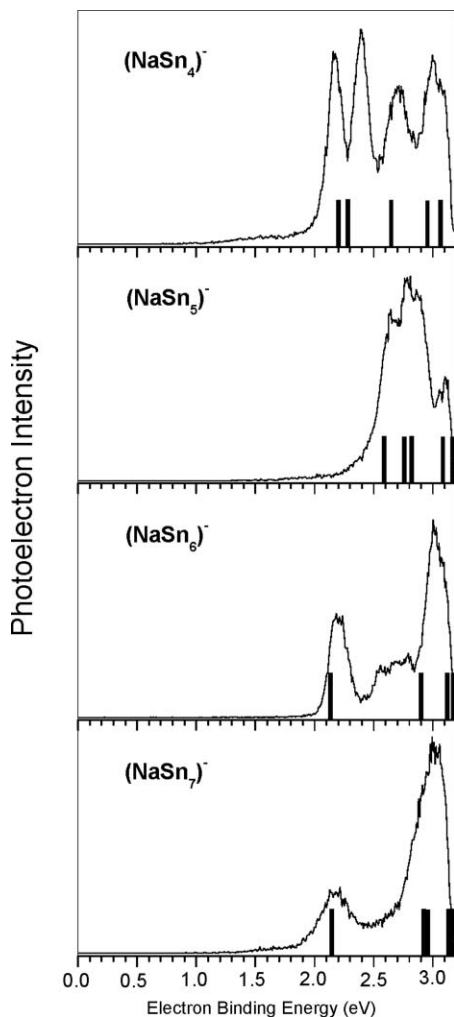


FIG. 3. Photoelectron spectra of $(\text{NaSn}_m)^-$, $m = 4-7$. The stick spectra indicate the predicted position of the vertical transitions from the singlet state of the anion to the doublet of the neutral.

corresponding neutral species. In the NaSn_n series, however, electron affinity values are similar in value except for case of NaSn_5 which has a higher electron affinity than the other members of this series.

TABLE I. Experimentally determined adiabatic electron affinities (AEA) and vertical detachment energies (VDE) for Na_nSn_m , $n = 0-4$, $m = 4-7$ clusters along with theoretical predictions for the same quantities. All values are given in eV.

Cluster	AEA (Expt.)	AEA (theory)	VDE (Expt.)	VDE (theory)
Sn_4	2.04	2.01	2.05	2.03
NaSn_4	2.10	1.90	2.17	2.20
Na_2Sn_4	1.55	1.60	1.67	1.79
Na_3Sn_4	1.38	1.48	1.51	1.62
Na_4Sn_4	0.90	0.57	0.99	1.02
NaSn_5	2.42	2.35	2.65	2.59
NaSn_6	2.12	2.07	2.20	2.13
NaSn_7	2.05	1.91	2.18	2.14

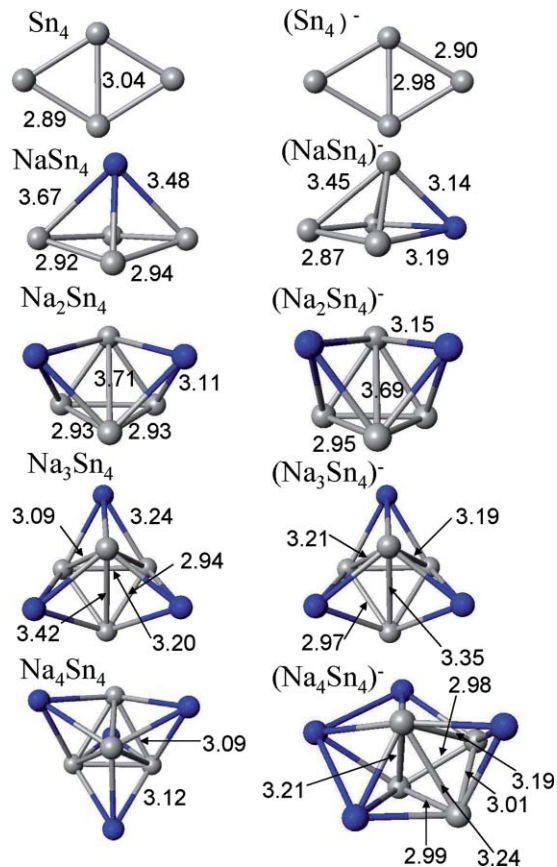


FIG. 4. The ground state geometries of the $(\text{Na}_n\text{Sn}_4)^-$, $n = 0-4$ anions and their corresponding neutrals. Black indicates sodium atoms, and gray indicates tin atoms. The bond lengths are in Å.

C. Ground state geometries

Figures 4 and 5 show the calculated ground state geometries of the neutral/anionic $\text{Na}_n\text{Sn}_4/(\text{Na}_n\text{Sn}_4)^-$ ($0 \leq n \leq 4$) and $\text{NaSn}_m/(\text{NaSn}_m)^-$ ($4 \leq m \leq 7$) species, respectively. First, consider the geometries of the $\text{Na}_n\text{Sn}_4/(\text{Na}_n\text{Sn}_4)^-$ ($0 \leq n \leq 4$) series. While Sn_4 and Sn_4^- are planar, the addition of a single sodium atom initiates the transformation to three dimensional structures for both $(\text{NaSn}_4)^-$ and NaSn_4 . Thereafter ($n \geq 2$), the geometries of both the $(\text{Na}_n\text{Sn}_4)^-$ and Na_nSn_4 series can be characterized as distorted tetrahedral Sn_4 cores decorated by sodium atoms. It is particularly instructive to compare the geometries of neutral Na_4Sn_4 and anionic $(\text{Na}_3\text{Sn}_4)^-$. Within our ability to reliably calculate bond distances, Na_4Sn_4 exhibits an almost perfectly tetrahedral Sn_4 core. Moreover, $(\text{Na}_3\text{Sn}_4)^-$ exhibits a Sn_4 core which, while slightly distorted due to the asymmetric arrangement of sodium atoms, is also close to being tetrahedral. Thus, the addition of either an alkali atom or an extra electron to neutral Na_3Sn_4 , [to form Na_4Sn_4 or $(\text{Na}_3\text{Sn}_4)^-$, respectively] produces species with similar Sn_4 core geometries, confirming that the primary role of alkali atoms in such species is to provide an additional electron to the Sn_4 motif. To further substantiate this, we carried out natural bond order (NBO) (charge) population analyses for both $(\text{Na}_3\text{Sn}_4)^-$ and Na_4Sn_4 . In $(\text{Na}_3\text{Sn}_4)^-$, the alkali atoms each had a valence charge of $+0.72$, while in Na_4Sn_4 , the sodium atoms each exhibited valence charges

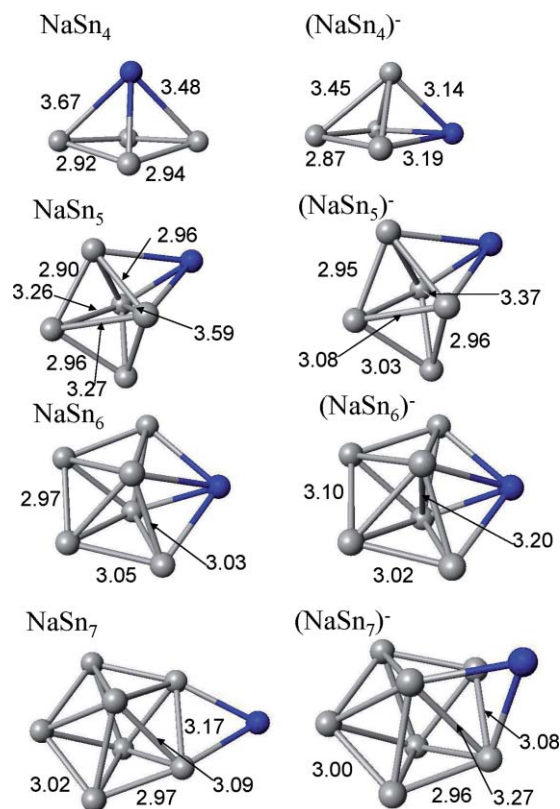


FIG. 5. The ground state geometries of the $(\text{NaSn}_m)^-$, $m = 4-7$ anions and their corresponding neutrals. Black indicates sodium atoms, and gray indicates tin atoms. The bond lengths are in Å.

of +0.82, indicating a substantial negative charge transfer to the Sn_4 motif in both cases. Next, consider the geometries of the $\text{NaSn}_n/(\text{NaSn}_n)^-$ ($4 \leq n \leq 7$) series. The geometry of the tin core of neutral NaSn_4 is nearly planar, while the geometry of the tin core in neutral and anionic NaSn_5 is a distorted trigonal bipyramidal. The neutral and anionic geometries of NaSn_6 can be characterized as pentagonal bipyramids in which the sodium atoms are a part of the pentagonal ring. The tin cores of the neutral and anionic NaSn_7 can themselves be described as pentagonal bipyramids, with each bonded to a sodium atom. In all cases, the ground states had the lowest spin multiplicity, i.e., odd electron systems were doublets while even electron systems were all singlets irrespective of the charged state.

D. Electronic properties

We have calculated a variety of electronic properties for the sodium/tin cluster systems studied herein. These properties include adiabatic detachment energies, vertical detachment energies, ionization potentials, photodetachment transition energies, HOMO-LUMO gaps, and the energies required to remove selected atoms from these clusters. The variation of these properties with cluster composition is presented in Figs. 6(a)–6(c).

Single atom removal energies are useful in characterizing relative stabilities. For members of the $(\text{Na}_n\text{Sn}_4)^-$ series, we calculated their sodium removal energies, $\text{Na R.E.}(\text{Na}_n\text{Sn}_m)^-$

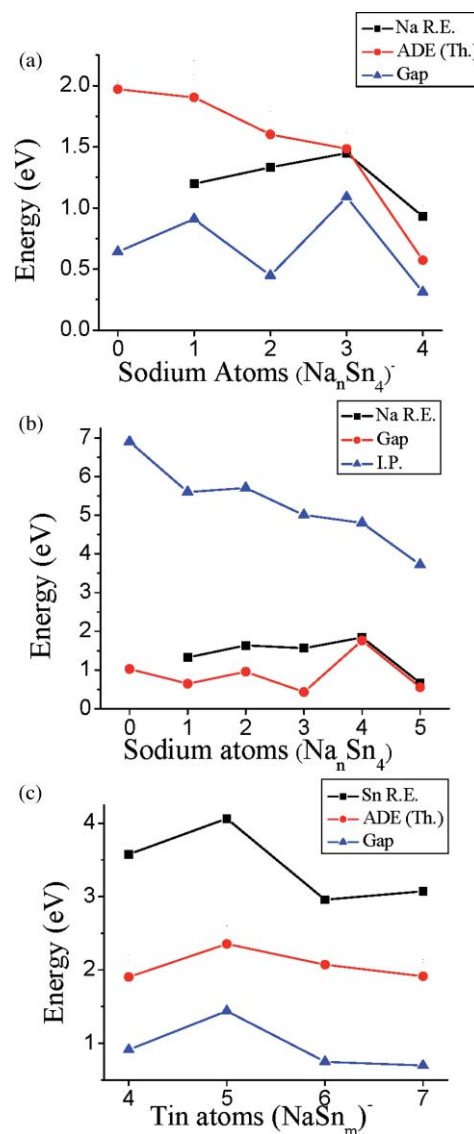


FIG. 6. (a) Properties of $(\text{Na}_n\text{Sn}_4)^-$, $n = 0-4$ (anions) as a function of n . (b) Properties of Na_nSn_4 , $n = 0-5$ (neutrals) as a function of n . (c) Properties of $(\text{NaSn}_m)^-$, $m = 4-7$ (anions) as a function of m . Na R.E. indicates removal energy for a sodium atom and Sn R.E. indicates the tin removal energy, ADE is the adiabatic detachment energy, I.P. is the ionization potential, and gap indicates HOMO-LUMO gap.

as defined in Eq. (1)

$$\text{Na R.E.}(\text{Na}_n\text{Sn}_m)^- = E(\text{Na}_{n-1}\text{Sn}_m)^- + E(\text{Na}) - E(\text{Na}_n\text{Sn}_m)^-. \quad (1)$$

The Na R.E. for neutral Na_nSn_4 was calculated in analogous fashion. For $(\text{NaSn}_n)^-$ clusters, the tin removal energy, Sn R.E. was calculated similarly

$$\text{Sn R.E.}(\text{Na}_n\text{Sn}_m)^- = E(\text{Na}_n\text{Sn}_{m-1})^- + E(\text{Sn}) - E(\text{Na}_n\text{Sn}_m)^-. \quad (2)$$

Single atom removal energies are plotted in Figs. 6(a)–6(c) for the $(\text{Na}_n\text{Sn}_4)^-$, Na_nSn_4 , and $(\text{NaSn}_m)^-$ cluster systems, respectively. Figure 6(a) shows that the Na R.E. energy is a maximum at $(\text{Na}_3\text{Sn}_4)^-$. This is consistent with characterizing $(\text{Na}_3\text{Sn}_4)^-$ as $(\text{Na}^+)_3(\text{Sn}_4)^{-4}$, where the three sodium atoms have donated their valence electrons to the tin core to form the highly stable $(\text{Sn}_4)^{-4}$ Zintl anion. Also, consistent

with this picture is the dramatic drop in Na R.E. in going from $n = 3$ to $n = 4$. Additional evidence for the stability of the $(\text{Sn}_4)^{-4}$ moiety is seen in the heightened sodium removal energy and the maximal HOMO-LUMO gap of neutral Na_4Sn_4 shown in Fig. 6(b). For the neutral Na_nSn_4 species, Fig. 6(b) also presents the calculated ionization potentials. In the $(\text{NaSn}_m)^-$ series [see Fig. 6(c)], the $m = 5$ ion has the largest tin removal energy (Sn R.E.) which correlates well with it having the highest intensity peak in the mass spectrum. Note that the tin removal (binding) energies [see Fig. 6(c)] generally display significantly higher values than the sodium binding energies [see Figs. 6(a) and 6(b)], possibly explaining the preponderance of tin rich clusters in the mass spectrum.

IV. DISCUSSION

In this work the experimentally derived parameters that can be quantitatively compared with the same theoretically computed parameters are electron affinities, vertical detachment energies, HOMO-LUMO gaps, and photodetachment transition energies, i.e., the photoelectron spectrum itself. Table I compares measured and calculated adiabatic electron affinities/adiabatic detachment energies. Figures 6(a) and 6(c) emphasize trends – showing variation of the theoretical vertical detachment energy values, point by point. Quantitative agreement between the theory and experiment is quite good, but agreement between the measured and predicted trends is excellent. For example, in the Na_nSn_4 series, both the photoelectron spectra (Fig. 2) and the theoretical calculations revealed decreasing electron affinity values as n increased from 1–4 (Fig. 6(a)) and a maximum in the value of the HOMO-LUMO gap at $n = 4$ (Fig. 6(b)). Also, in the case of Sn_4 , we had the work of others with which to compare. Most previous determinations^{34–37} of its adiabatic electron affinity as well as our own measurement found it to be 2.04 eV, while our calculations predicted it to be 2.03 eV.

The most compelling comparison between experiment and theory, however, involves modeling the actual photoelectron spectra, i.e., calculating the photodetachment transition energies for each species. In this study theory accurately modeled almost every electronic transition observed in the experimental photoelectron spectra (see predicted stick spectra in Figs. 2 and 3). Good agreement between an experimentally observed spectrum and its theoretically predicted stick spectrum suggests that other electronically sensitive parameters, such as geometry, have also been accurately calculated, thus validating the theoretical computations. In this sense, the photoelectron spectrum of an anion provides an indirect fingerprint of the anion's geometry as well as that of its neutral counterpart, albeit at the structure of the anion.

The measured versus predicted HOMO-LUMO gaps in a given system are best compared by examining the energy spacing between the transitions having the lowest and the next highest EBE values in the calculated stick spectrum. In the spectrum of $(\text{Na}_4\text{Sn}_4)^-$, the species with the largest HOMO-LUMO gap in this study, the measured gap is nominally ~ 1 eV, while the spacing between the stick transitions is 1.0 eV. Calculated gaps for the ground state geometries of

neutral Na_4Sn_4 and its anion, Na_4Sn_4^- are somewhat higher and lower, respectively [see Figs. 6(a) and 6(b)]. The difference in the gap measured by photodetaching Na_4Sn_4^- and the calculated gap for Na_4Sn_4 is mostly due to two factors. The gap that we measure in this way is the gap of the neutral at the geometry of the anion, not the gap of the neutral at its ground state geometry which is the quantity calculated. Interestingly, the band gap of the β -Na/Sn solid is $E_g = 0.74$ eV.²⁵ Note that the band gap energy of the cluster assembled solid is affected by the nature of the counter-cation as well as the architecture of the assembled solid.^{38,39} Also since the HOMO-LUMO gap is dependent on charge transfer and since the charge transfer at the anion geometry and at the neutral geometry is different, the gap are reduced in the anion geometry. Below, we consider what can be learnt from each of the major sodium/tin cluster stoichiometries considered in this study.

A. $\text{NaSn}_4/(\text{NaSn}_4)^-$

The neutral cluster, NaSn_4 could be viewed as $\text{Na}^+(\text{Sn}_4)^-$, but in its anion, where does the excess electron go? In the anions of alkali halides⁴⁰ and ammonium halides,⁴¹ there is ample evidence to indicate that $(\text{M}^+\text{X}^-)^-$ is best described as M^0X^- and not as M^+X^{2-} . Polyatomic assemblies of tin and other heavy group IV elements, however, are known to be able to support multiple negative charges, i.e., to form Zintl anions. In $(\text{NaSn}_4)^-$, the sodium atom contributes one additional electron to the negative charge already present on the cluster anion, and that could provide the tin moiety with two excess electrons. In that case $(\text{NaSn}_4)^-$ would be best described as $\text{Na}^+(\text{Sn}_4)^{2-}$ and not as $\text{Na}^0(\text{Sn}_4)^-$. Which one actually occurs depends on the relative stability of $(\text{Sn}_4)^{2-}$ versus $(\text{Sn}_4)^-$ in conjunction with their particular sodium environments. Our calculations show the structure of $(\text{NaSn}_4)^-$ to be a $(\text{Sn}_4)^{2-}$ tetrahedron capped by a Na^+ cation, while the structure of $(\text{Sn}_4)^-$ is planar. This assignment is supported by the observation that while the photoelectron spectrum of $(\text{Sn}_4)^-$ is very similar to that of $(\text{Si}_4)^-$,^{42–44} the photoelectron spectrum of $(\text{NaSn}_4)^-$ is dramatically different from that of $(\text{NaSi}_4)^-$,⁴⁵ suggesting that they exhibit different bonding and structures. This is consistent with the fact that tin forms Zintl-like anions and silicon does not. It is also interesting to note that the proper description of $(\text{KAl}_3)^-$, i.e., $[\text{K}^+(\text{Al}_3)^-]^-$, is $\text{K}^0(\text{Al}_3)^-$ and not $\text{K}^+(\text{Al}_3)^{2-}$, in large part because singly charged $(\text{Al}_3)^-$ is itself a closed shell species.¹⁷

B. $\text{Na}_2\text{Sn}_4/(\text{Na}_2\text{Sn}_4)^-$

The addition of a second sodium atom to $(\text{NaSn}_4)^-$ to form $(\text{Na}_2\text{Sn}_4)^-$ gives the anionic cluster an odd number of electrons, reducing its stability relative to $(\text{NaSn}_4)^-$. This is reflected in the diminished mass spectral intensity of $(\text{Na}_2\text{Sn}_4)^-$ as seen in Fig. 1 and the lowered electron affinity value of Na_2Sn_4 as seen in both Figs. 2 and 6(a). Two Na atoms stabilize the tetrahedral Sn_4 core geometry in both neutral and anionic sodium/tin cluster species.

C. $\text{Na}_3\text{Sn}_4/(\text{Na}_3\text{Sn}_4)^-$

$(\text{Na}_3\text{Sn}_4)^-$ is of special interest because it can be described as $(\text{Na}^+)_3(\text{Sn}_4)^{-4}$, and its $(\text{Sn}_4)^{-4}$ moiety is an established Zintl anion. The enhanced stability of $(\text{Na}_3\text{Sn}_4)^-$ is reflected in it having the highest sodium removal energy in the $(\text{Na}_n\text{Sn}_4)^-$ series [see Fig. 6(a)]. The origin of the stability of $(\text{Sn}_4)^{-4}$ can be described in two ways. The simplest is to realize that the addition of four extra electrons to the covalent Sn_4 cluster satisfies the octet rule, i.e., $(\text{Sn}_4)^{-4}$ is a closed shell. As shown in Fig. 7(a), where the one-electron energy levels are plotted as a function of the number of sodium atoms, there is very little mixing between the widely separated s and p states in $(\text{Na}_3\text{Sn}_4)^-$. For the purpose of counting electrons, eight electrons come from the p -orbitals of the four tin atoms, eight more electrons derive from the deeper s -orbitals of the same four tin atoms, and four electrons are associated with the net negative charge on $(\text{Sn}_4)^{-4}$. In its tetrahedral geometry, $(\text{Sn}_4)^{-4}$ has six Sn–Sn bonds, requiring 12 bonding electrons. With the eight s -orbital electrons acting as four lone pairs, each tin atom satisfies the octet rule, and this underpins the high stability of $(\text{Sn}_4)^{-4}$. A second explanation for the stability of $(\text{Sn}_4)^{-4}$ invokes spherical aromaticity.⁴⁶ The most stable p molecular orbital in the $(\text{Sn}_4)^{-4}$ moiety in Na_3Sn_4^- has two π electrons as can be seen in a plot of the charge density. This is consistent with the $2(N+1)^2$ (Hirsch's) rule, where $N=0$.

Also of note, our calculations show that the $(\text{Sn}_4)^{-4}$ moiety within $(\text{Na}_3\text{Sn}_4)^-$ is strongly distorted from an ideal tetrahedral structure (see Fig. 4). These distortions are consistent with the photoelectron spectrum of $(\text{Na}_3\text{Sn}_4)^-$ in that the spectral feature between $\text{EBE} = 2.0\text{--}2.5$ eV is broad. This suggests that a lifting of the tetrahedral symmetry for the

$(\text{Sn}_4)^{-4}$ core has occurred, since a pure tetrahedral symmetry would most likely have resulted in a narrower peak. Thus, asymmetrically located sodium cations distort the T_d symmetry of the tin atom cage in $(\text{Na}_3\text{Sn}_4)^-$. Nevertheless, the electronic structure of $(\text{Sn}_4)^{-4}$ is still recognizable as gauged by the large HOMO-LUMO gap in $(\text{Na}_3\text{Sn}_4)^-$ [see Fig. 6(a)]. Thus, the gain in electronic stability is robust even in the face of external distortion.

D. $\text{Na}_4\text{Sn}_4/(\text{Na}_4\text{Sn}_4)^-$

$(\text{Na}_4\text{Sn}_4)^-$ is the anion of the fundamental unit of the 1:1 Na:Sn Zintl phase, $(\text{Na}^+)_4(\text{Sn}_4)^{-4}$, and since $(\text{Sn}_4)^{-4}$ is a closed shell, so is net-neutral $(\text{Na}^+)_4(\text{Sn}_4)^{-4}$. This species and its anion, $(\text{Na}_4\text{Sn}_4)^-$ are reminiscent of KAl_{13} and its anion, $(\text{KAl}_{13})^-$.¹⁷ Both neutral species are closed shells, and both are significantly ionically bonded entities in which alkali cations interact with negatively charged polyatomic aggregates, *viz.*, $\text{K}^+(\text{Al}_{13})^-$ and $(\text{Na}^+)_4(\text{Sn}_4)^{-4}$. Moreover, within their immediate homologous series, both the mass spectral intensities of their anions and the electron affinities of their neutral forms exhibit minimal values, while the HOMO-LUMO gaps of their neutrals display maximal values. This combination of properties is a hallmark of closed shell neutrals and their anions, and these characteristics are directly observed in the mass spectrum shown in Fig. 1 and the photoelectron spectrum of $(\text{Na}_4\text{Sn}_4)^-$ presented in Fig. 2. These properties are also reflected through our calculations; the ADE of $(\text{Na}_4\text{Sn}_4)^-$ (the electron affinity of Na_4Sn_4) is a minimum, and the HOMO-LUMO gap of Na_4Sn_4 is a maximum (see Fig. 6). Additionally, the calculations show that the sodium removal energy for Na_4Sn_4 is the highest in its homologous series.

Our calculations show that the geometry of $(\text{Sn}_4)^{-4}$ within neutral Na_4Sn_4 differs negligibly from the perfect tetrahedral symmetry, reflecting the closed shell character and tetrahedral symmetry of $(\text{Sn}_4)^{-4}$. Our calculations also show that this inner tin cage resides within a tetrahedral cage of sodium cations, rotated so that the sodium cations sit above the tetrahedral faces of the tin cage. In the case of $(\text{Na}_4\text{Sn}_4)^-$, however, inner tin cage loses its perfect tetrahedral symmetry with one face of the distorted tin tetrahedron left empty and with one of the sodium cations interacting with two tin and two sodium atoms as shown in Fig. 4. According to our calculations, the tetrahedral geometry $(\text{Na}_4\text{Sn}_4)^-$ lies 0.12 eV above the ground state and has a vertical detachment energy of 0.56 eV. The distorted geometry shown in Fig. 4 is predicted to have a VDE of 1.02 eV, and this is in good agreement with our photoelectron spectrum of $(\text{Na}_4\text{Sn}_4)^-$. Note that the experimental difference of 0.09 eV between the VDE and ADE in Table I is less than the calculated difference of 0.45 eV. Since the atomic structure in the ground state of the neutral cluster is different from the anion, it is possible that the calculated neutral ground state is not accessible in the experiment. One imagines that the structure of $(\text{Na}_4\text{Sn}_4)^-$ is related to the placement of the excess electron in $(\text{Na}^+)_4(\text{Sn}_4)^{-4}$. Since $(\text{Sn}_4)^{-4}$ is a closed shell, the excess electron can not go there and must instead reside on the sodium cation (or cations) to

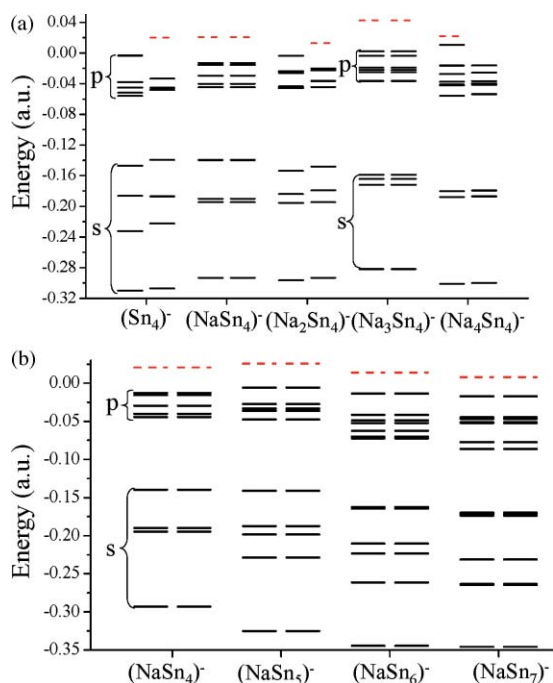


FIG. 7. (a) The one electron levels for the majority and minority spins in $(\text{Na}_n\text{Sn}_4)^-$, $n=0\text{--}4$ anions. (b) The one electron levels for the majority and minority spins in $(\text{NaSn}_m)^-$, $m=4\text{--}7$ anions. Continuous lines represent the filled states while the dotted lines represent unfilled levels.

form $[(\text{Na}^0)(\text{Na}^+)_3(\text{Sn}_4)^{-4}]$. In fact, the calculated structure is most consistent with the excess electron going to a single sodium cation to form its neutral atom, i.e., to the outlying sodium that interacts with two tin and two sodium atoms. An analysis of the frontier orbitals confirms this analysis as the HOMO is found to be mostly localized on the bridging Na.

E. $\text{NaSn}_5/(\text{NaSn}_5)^-$

$(\text{NaSn}_5)^-$ distinguishes itself among the species of the $(\text{NaSn}_m)^-$, $m = 4-7$ series. In the mass spectrum, $(\text{NaSn}_5)^-$ is observed to have the highest ion intensity, and in its photoelectron spectrum, NaSn_5 is seen to have a higher electron affinity than the other species in the series by ~ 0.5 eV. According to our calculations, $(\text{NaSn}_5)^-$ has the largest anion HOMO-LUMO gap, the largest ADE value (i.e., the largest electron affinity), and the largest tin removal energy among the species in the $(\text{NaSn}_m)^-$ series. All of this indicates that $(\text{NaSn}_5)^-$ possesses high electronic stability. The high stability of $(\text{NaSn}_5)^-$ derives from it being a Wade-Mingos^{47,48} cluster with 12 p ($2n + 2$ where $n = 5$) electrons. In turn, this implies a closo trigonal bipyramidal structure for $(\text{Sn}_5)^{-}$, and indeed, as shown in Fig. 5, this is essentially the geometry that we find in our calculations for the Sn_5^- moiety within $(\text{NaSn}_5)^-$. The other members of the series also have interesting structures. The geometry of $(\text{NaSn}_6)^-$ is distorted from octahedral geometry by the presence of the sodium atom. This is related to the spherical anti-aromaticity of the $(\text{Sn}_6)^{-2}$ core whose electronic structure is very sensitive to the symmetry of the cluster.⁴⁹ Also, the geometry of the $(\text{NaSn}_7)^-$ cluster is slightly distorted from its ideal pentagonal bipyramidal structure. Nevertheless, the $(\text{NaSn}_5)^-$ cluster shows the least distortion from the expected closo geometry; this goes hand in hand with its high electronic stability.

The high stability of $(\text{NaSn}_5)^-$ also suggests that $(\text{Sn}_5)^{2-}$ may be a Zintl anion and that $(\text{NaSn}_5)^-$ is best characterized as $\text{Na}^+(\text{Sn}_5)^{2-}$. This is supported by work in the condensed phase where $[\text{CryptNa}]_2\text{Sn}_5$ was synthesized and determined to have a trigonal bipyramidal structure⁵⁰ and where NaSn_5 was found to be the most tin-rich phase of the sodium/tin system in the solid.⁵¹ Thus, our observation of the $(\text{NaSn}_5)^-$ magic cluster anion in the gas phase mimics the occurrence of the $(\text{Sn}_5)^{2-}$ Zintl anion in the condensed phase.

V. CONCLUSIONS

By utilizing a combination of mass spectroscopy, anion photoelectron spectroscopy, and theoretical calculations, we have determined the energetic properties and geometrical structures of several $(\text{Na}_n\text{Sn}_m)^-/\text{Na}_n\text{Sn}_m$ cluster systems, finding excellent agreement between experiment and theory. Strong evidence was presented for the presence of the two Zintl anion moieties, $(\text{Sn}_4)^{4-}$ and $(\text{Sn}_5)^{2-}$ in these gas phase cluster systems. Some of the electronically stable, gas phase clusters studied here are prototypical units of Zintl phases which are well known in condensed phases. The viability of Zintl phase systems in both the gas and the condensed phases is a precedent for efforts to form cluster assembled materials

from systems which share analogous bonding principles, e.g., KAl_{13} .

ACKNOWLEDGMENTS

K.H.B. thanks the Division of Materials Sciences and Engineering, Office of Basic Energy Sciences, U.S. Department of Energy (DOE) for support of the experimental part of this work under Grant Number DE-FG02-09ER46558. A.C.R. and S.N.K. acknowledge support from the Department of Energy (DOE).

- ¹E. Zintl, *Angew. Chem.* **52**, 1 (1939).
- ²J. D. Corbett, *Chem. Rev.* **85**, 383 (1985).
- ³*Chemistry, Structure, and Bonding of Zintl Phases and Ions*, edited by S. M. Kauzlarich (Wiley VCH, Berlin, 1996).
- ⁴J. D. Corbett, *Structure Bonding* **87**, 157 (1997).
- ⁵R. W. Farley and A. W. Castleman, Jr., *J. Am. Chem. Soc.* **111**, 2734 (1989).
- ⁶R. W. Farley and A. W. Castleman, Jr., *J. Chem. Phys.* **92**, 1790 (1990).
- ⁷R. G. Wheeler, K. Lai-Hing, W. L. Wilson, J. D. Allen, R. B. King, and M. A. Duncan, *J. Am. Chem. Soc.* **108**, 8101 (1986).
- ⁸M. B. Bishop, K. Lai-Hing, P. Y. Cheng, M. Peschke, and M. A. Duncan, *J. Phys. Chem.* **93**, 1566 (1989).
- ⁹X. Li, A. E. Kuznetsov, H.-F. Zhang, A. I. Boldyrev, and L. S. Wang, *Science* **291**, 859 (2001).
- ¹⁰A. Kuznetsov, A. I. Boldyrev, X. Li, and L.-S. Wang, *J. Am. Chem. Soc.* **123**, 8825 (2001).
- ¹¹E. N. Esenturk, J. Fettinger, Y. F. Lam, and B. Eichhorn, *Angew. Chem., Int. Ed.* **43**, 2132 (2004).
- ¹²E. N. Esenturk, J. Fettinger, and B. Eichhorn, *Chem. Commun.* **247** (2005).
- ¹³S. N. Khanna and P. Jena, *Phys. Rev. B* **51**, 13705 (1995).
- ¹⁴K. Hoshino, K. Watanabe, Y. Konishi, T. Taguwa, A. Nakajima, and K. Kaya, *Chem. Phys. Lett.* **231**, 499 (1994).
- ¹⁵K. Koyasu, M. Akutsu, J. Atoke, M. Mitsui, and A. Nakajima, *Chem. Phys. Lett.* **421**, 534 (2006).
- ¹⁶C. Ashman, S. N. Khanna, and M. R. Pederson, *Phys. Rev. B* **66**, 193408 (2002).
- ¹⁷W.-J. Zheng, O. C. Thomas, T. P. Lippa, S.-J. Xu, and K. H. Bowen, *J. Chem. Phys.* **124**, 144304 (2006).
- ¹⁸L.-F. Cui, X. Huang, L.-M. Wang, D. Y. Zubarev, A. I. Boldyrev, J. Li, and L.-S. Wang, *J. Am. Chem. Soc.* **128**, 8390 (2006).
- ¹⁹L.-F. Cui, X. Huang, L.-M. Wang, J. Li, and L.-S. Wang, *J. Phys. Chem. A* **110**, 10169 (2006).
- ²⁰P. A. Clayborne, U. Gupta, A. C. Reber, J. J. Melko, S. N. Khanna, and A. W. Castleman, Jr., *J. Chem. Phys.* **133**, 134302 (2010).
- ²¹A. W. Castleman, Jr., S. N. Khanna, A. Sen, A. C. Reber, M. Qian, K. M. Davis, S. J. Peppernick, A. Ugrinov, and M. D. Merritt, *Nano Lett.* **7**, 2734 (2007).
- ²²A. Hirsch, Z. F. Chen, and H. J. Jiao, *Angew. Chem., Int. Ed.* **40**, 2834 (2001).
- ²³B. Wang, L. M. Molina, M. J. Lopez, A. Rubio, J. A. Alonso, and M. J. Stott, *Ann. Phys.* **7**, 107 (1998).
- ²⁴B. Wang, M. J. Stott, and J. A. Alonso, *Phys. Rev. B* **65**, 045410 (2002).
- ²⁵J. Fortner, M.-L. Saboungi, and J. E. Enderby, *Phys. Rev. Lett.* **74**, 1415 (1995).
- ²⁶F. Springelkamp, R. A. de Groot, W. Geertsma, W. van der Lugt, and F. M. Mueller, *Phys. Rev. B* **32**, 2319 (1985).
- ²⁷M.-L. Saboungi, J. Fortner, W. S. Howells, and D. L. Price, *Nature (London)* **365**, 237 (1993).
- ²⁸O. C. Thomas, W. J. Zheng, and K. H. Bowen, *J. Chem. Phys.* **114**, 5514 (2001).
- ²⁹W. Kohn and L. J. Sham, *Phys. Rev.* **140**, A1133 (1965).
- ³⁰J. P. Perdew, K. Burke, and M. Ernzerhof, *Phys. Rev. Lett.* **77**, 3865 (1996).
- ³¹M. R. Pederson and K. A. Jackson, *Phys. Rev. B* **41**, 7453 (1990).
- ³²K. Jackson and M. R. Pederson, *Phys. Rev. B* **42**, 3276 (1990).
- ³³D. Porezag, K. A. Jackson, and M. R. Pederson, *Phys. Rev. A* **60**, 2840 (1999).
- ³⁴G. Gantefoer, M. Gausa, K. H. Meiwes-Broer, and H. O. Lutz, *Z. Phys. D: At., Mol. Clusters* **12**, 405 (1989).

- ³⁵V. D. Moravec, S. A. Klopčič, and C. C. Jarrold, *J. Chem. Phys.* **110**, 5079 (1999).
- ³⁶Y. Negishi, H. Kawamata, A. Nakajima, and K. Kaya, *J. Electron Spectrosc. Relat. Phenom.* **106**, 117 (2000).
- ³⁷L.-F. Ciu, L.-M. Wang, and L.-S. Wang, *J. Chem. Phys.* **126**, 064505 (2007).
- ³⁸M. Qian, A. C. Reber, A. Ugrinov, N. K. Chaki, S. Mandal, H. M. Saavedra, S. N. Khanna, A. Sen, and P. Weiss, *ACS Nano* **4**, 235 (2010).
- ³⁹N. K. Chaki, S. Mandal, A. C. Reber, M. Qian, H. M. Saavedra, P. S. Weiss, S. N. Khanna, and A. Sen, *ACS Nano* **4**, 5813 (2010).
- ⁴⁰T. M. Miller, D. G. Leopold, K. K. Murray, and W. C. Lineberger, *J. Chem. Phys.* **85**, 2368 (1986).
- ⁴¹S. N. Eustis, D. Radisic, K. H. Bowen, R. A. Bachorz, M. Haranczyk, G. K. Schenter, and M. Gutowski, *Science* **319**, 93 (2008).
- ⁴²O. Cheshnovsky, S. H. Yang, C. L. Pettiette, M. J. Craycraft, Y. Liu, and R. E. Smalley, *Chem. Phys. Lett.* **138**, 119 (1987).
- ⁴³M. R. Nimlos, L. B. Harding, and G. B. Ellison, *J. Chem. Phys.* **87**, 5116 (1987).
- ⁴⁴T. N. Kitsopoulos, C. J. Chick, A. Weaver, and D. M. Neumark, *J. Chem. Phys.* **93**, 6108 (1990).
- ⁴⁵R. Kishi, H. Kawamata, Y. Negishi, S. Iwata, A. Nakajima, and K. Kaya, *J. Chem. Phys.* **107**, 10029 (1997).
- ⁴⁶A. Hirsch, Z. Chen, and H. Jiao, *Angew. Chem., Int. Ed.* **39**, 3915 (2000).
- ⁴⁷K. Wade, *Adv. Inorg. Chem. Radiochem.* **18**, 1 (1976).
- ⁴⁸D. M. P. Mingos, *Chem. Soc. Rev.* **15**, 31 (1986).
- ⁴⁹R. B. King, T. Heine, C. Corminboeuf, and P. V. R. Schleyer, *J. Am. Chem. Soc.* **126**, 430 (2004).
- ⁵⁰P. A. Edwards and J. D. Corbett, *Inorg. Chem.* **16**, 903 (1977).
- ⁵¹T. F. Fassler and C. Kronseder, *Angew. Chem., Int. Ed.* **37**, 1571 (1998).